ACS APPLIED MATERIALS & INTERFACES

www.acsami.org

Research Article

Laser-Engineered Microcavity Surfaces with a Nanoscale Superhydrophobic Coating for Extreme Boiling Performance

Matic Može,* Matej Senegačnik, Peter Gregorčič, Matej Hočevar, Matevž Zupančič,* and Iztok Golobič

Cite This: *ACS Appl. Mater. Interfaces* 2020, 12, 24419−24431

Read Online

ACCESS | Metrics & More | Article Recommendations | Supporting Information

ABSTRACT: Functionalized interfaces enhancing phase-change processes have immense applicability in thermal management. Here, a methodology for fabrication of surfaces enabling extreme boiling heat transfer performance is demonstrated, combining direct nanosecond laser texturing and chemical vapor deposition of a hydrophobic fluorinated silane. Multiple strategies of laser texturing are explored on aluminum with subsequent nanoscale hydrophobization. Both superhydrophilic and superhydrophobic surfaces with laser-engineered microcavities exhibit significant enhancement of the pool boiling heat transfer. Surfaces with superhydrophobic microcavities allow for enhancements of a heat transfer coefficient of over 500%. Larger microcavities with a mean diameter of 4.2 μm, achieved using equidistant laser scanning separation, induce an early transition into the favorable nucleate boiling regime, while smaller microcavities with a mean diameter of 2.8 μm, achieved using variable separation, provide superior performance at high heat fluxes. The enhanced boiling performance confirms that the Wenzel wetting regime is possible during boiling on apparently superhydrophobic surfaces. A notable critical heat flux enhancement is demonstrated on superhydrophobic surfaces with an engineered microstructure showing definitively the importance and concomitant effect of both the surface wettability and topography for enhanced boiling. The fast, low-cost, and repeatable fabrication process has great potential for advanced thermal management applications.

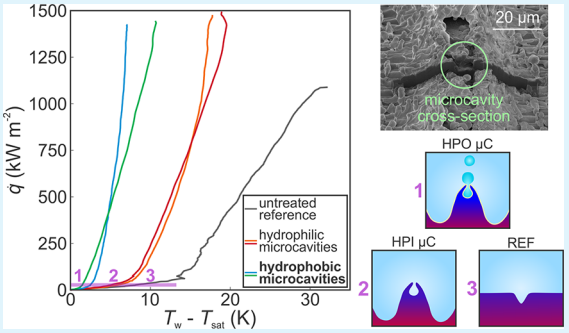

KEYWORDS: *surface functionalization, surface engineering, hydrophobic surfaces, pool boiling, laser texturing*

1. INTRODUCTION

Emergence of new information technologies including artificial intelligence, internet of things, and big data requires a powerful computer infrastructure, which is a major consumer of electricity and is projected to grow at a rate of 10% per year.[1] Development of high-performance electronics and their miniaturization in the last few decades resulted in increased requirements for their efficient cooling with the energy consumption for cooling purposes representing 30−55% of the total energy use.[2,3] Since several hundred kilowatts per square meter needs to be dissipated from certain components, development and implementation of enhanced cooling methods is crucial. Phase-change heat transfer via boiling has been proven to be one of the best solutions as it can reach extremely high values of the heat transfer coefficient (defined as the ratio between the heat flux and the temperature difference between the surface and the fluid), which is used to quantify the heat transfer intensity. Furthermore, boiling heat transfer is already utilized in critical applications such as cooling of nuclear reactor fuel rods and for nuclear accident management.[4] With the recent pressure to achieve higher energy efficiency and better utilization of renewable energy sources, emerging technologies including electric vehicles, their batteries, and renewable energy power generation machinery will also need to consider using boiling heat transfer for cooling purposes.[5]

While boiling is one of the most intense cooling processes with heat transfer coefficients, several orders of magnitude higher in comparison with natural or forced convection, there is still room for its enhancement with most efforts aimed at enhancing the properties of the boiling surface (i.e., its wettability, microstructure, porosity etc.). The microstructure of the surface significantly influences the nucleate boiling heat transfer as bubbles preferably grow from defects (cavities) on the surface. Therefore, the presence of an abundance of suitable microcavities is important for efficient boiling heat transfer as it enables an early transition from the natural convection regime without phase change into the nucleate boiling regime with much higher heat transfer intensity. Wettability of the boiling surface also significantly affects the heat transfer performance with poorly wettable (hydrophobic)

Received: January 27, 2020
Accepted: April 30, 2020
Published: April 30, 2020

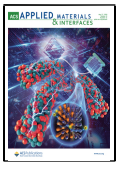

surfaces typically exhibiting lower critical heat flux (CHF; the upper limit of the desirable nucleate boiling regime), making such surfaces less suitable for practical use.[6] Especially, superhydrophobic surfaces usually exhibit unfavorable heat transfer properties in the fully developed nucleate boiling regime with an early transition into film boiling.[7−12] On the contrary, (super)hydrophilic and porous surfaces tend to exhibit increased CHF but overall higher superheats due to the higher energy barrier for nucleation.[13−15] While a high CHF might represent an additional safety margin in some applications, high performance at somewhat lower heat fluxes in terms of very high heat transfer coefficients is more important in many applications utilizing boiling heat transfer as a cooling method.[4,16,17]

The appearance of the Cassie−Baxter wetting state on superhydrophobic surfaces will universally result in an early transition into film boiling accompanied by a massive surface temperature increase and subsequent substantial reduction of the heat transfer intensity.[18] If the Wenzel wetting regime is achieved, then an enhancement of the heat transfer coefficient (and with that, the heat transfer intensity) will be present, although without a major enhancement of the CHF, which was recently shown by Allred et al.[18] Therefore, significantly increasing both the critical heat flux and the heat transfer coefficient using superhydrophobic boiling surfaces remains a challenge.

Several methods for micro- and nanotexturing of the boiling surface have been shown to enhance boiling heat transfer,[19,20] yet few of these methods are truly scalable and straightforward while still offering great boiling enhancements.[21−23] Herein lies the advantage of laser texturing, which can be utilized to modify the micro- and nanostructure of the surface, its chemical composition, and morphology,[24,25] all of which significantly affect boiling heat transfer. To this effect, Kruse et al.[26] produced multiscale structures on stainless steel using a femtosecond laser, while Nirgude and Sahu[27] applied nanosecond laser texturing to functionalize copper surfaces. Zupančič et al.[28] and Voglar et al.[29] used a nanosecond laser to produce microcavities on a stainless steel surface, which were proven to greatly enhance the boiling heat transfer by serving as active nucleation sites from which bubbles prefer to form, while Može et al.[30] demonstrated that this approach can also be applied to copper. Gregorčič et al.[23] have shown that such surfaces offer similar enhancements using different (pure) coolants with significantly different properties, while Zakšek et al.[31] proved that they also work for binary fluid mixtures. Even though (solely) laser-textured boiling surfaces are showing favorable heat transfer enhancement results, extremely high heat transfer coefficients (>100 kW m^{-2} K^{-1}) have not been recorded on them to date.

Efficient thermal management using boiling heat transfer relies on low surface superheat and high values of both the critical heat flux and the heat transfer coefficient. Typical surface modifications such as wettability alteration rarely achieve preferable values of all three parameters at the same time and require sacrificing at least one aspect of boiling performance, outlining the need for an innovative approach to boiling enhancement. This study presents a low-cost, fast, and reliable method of producing superhydrophobic aluminum surfaces for extreme pool boiling performance by combining laser surface functionalization with chemical vapor deposition (CVD) of a hydrophobic fluorinated silane. Direct nanosecond laser texturing is used to induce microcavities, and different laser texturing strategies are investigated with subsequent hydrophobization of selected surfaces. SEM imaging is used to analyze the surface morphology and to evaluate the size distribution of microcavities. Pool boiling tests using water are conducted to evaluate the boiling heat transfer performance, and the mechanism of heat transfer enhancement is proposed and discussed. Superhydrophobic coating ensures transition into the nucleate boiling regime at surface temperatures only slightly above the saturation temperature of water without the appearance of the Cassie−Baxter regime (i.e., without immediate transition into undesirable film boiling), while laser-induced microcavities enable effective nucleation throughout the nucleate boiling regime. We convincingly show that superhydrophobic surfaces, which allow the establishment of the Wenzel wetting regime and also have an appropriate microstructure, can actually increase the CHF, which contradicts the current understanding of boiling heat transfer performance on poorly wettable surfaces. The developed surfaces provide sacrifice-free boiling performance enhancement and offer both increased cooling system safety and highly efficient cooling with heat transfer coefficients in an excess of 200 kW m^{-2} K^{-1}.

2. RESULTS AND DISCUSSION

2.1. Laser-Functionalized Aluminum Surfaces. Irradiation of a solid material with laser light induces changes in its morphology, topography, and chemistry due to the temperature increase and accompanying phase-change phenomena. One of the possible surface features resulting from laser texturing is microcavities, which form through ablation and melting (followed by solidification) of the material using pulse fluences, significantly higher than the threshold fluence for ablation. For the used aluminum alloy, the ablation threshold was determined, as described in ref.,[32] and equals approximately 3 J cm^{-2}. The rapid melting and vaporization of the material results in recoil pressure exceeding the surface tension of the liquefied material, which in turn induces hydrodynamic motion of the molten material toward the sides of each laser beam trace.[23,33] A graphical explanation of the microcavity formation process is shown in Figure 1. For the microcavities to form successfully and reliably, the laser texturing parameters (especially the texturing pattern, laser pulse overlap, and pulse fluence) need to be tailored to the individual material.[32] Furthermore, only a narrow range of lateral separation values between parallel laser beam scanning lines produces micro-

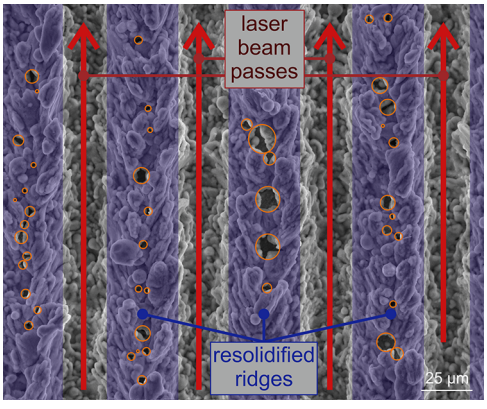

Figure 1. Graphical explanation of the formation process of laser-induced microcavities.

https://dx.doi.org/10.1021/acsami.0c01594
ACS Appl. Mater. Interfaces 2020, 12, 24419−24431

Table 1. List of Tested Surfaces

surface name	description	fabrication process	apparent CA after fabrication	apparent CA after boiling
REF	untreated reference surface	none	76°	90°
HPO smooth	smooth hydrophobic surface	CVD	124°	76°
HPO FT	superhydrophobic fully textured surface[a]	laser texturing + CVD	>150°	133°
HPI FT	superhydrophilic fully textured surface	laser texturing	<1°	nonuniform droplet spreading
HPO VS 1	superhydrophobic surface with microcavities[a]	laser texturing + CVD	>150°	>150°
HPO VS 2	superhydrophobic surface with microcavities[a]	laser texturing + CVD	>150°	143°
HPO VS 3	superhydrophobic surface with microcavities[a]	laser texturing + CVD	>150°	141°
HPO ES 1	superhydrophobic surface with microcavities[a]	laser texturing + CVD	>150°	144°
HPO ES 2	superhydrophobic surface with microcavities[a]	laser texturing + CVD	>150°	143°
HPI VS	superhydrophilic surface with microcavities	laser texturing	<1°	nonuniform droplet spreading
HPI ES	superhydrophilic surface with microcavities	laser texturing	<1°	nonuniform droplet spreading

[a]roll-off angle, <5°.

cavities.[23] Therefore, it is beneficial to use variable separation to cover the entire viable range, which should ensure reliable formation of microcavities. On the other hand, an equidistant separation corresponding to the value producing a lot of microcavities with appropriate diameters for early nucleation could be employed as a speculative approach to possibly generate a higher total number of microcavities. However, this comes with both the risk of generating no suitable microcavities for boiling if the selected line separation turns out to be inappropriate in combination with the selected laser texturing parameters and the possibility of lower boiling performance due to an overall narrower range of microcavity diameters. Both approaches were tested in this study. Additional details are available in Section S5 where Figure S19 shows the relationship between the scanning line separation and microcavity formation for a specific set of laser texturing parameters.

The tested surfaces are listed in Table 1. Best-performing surfaces were fabricated and tested multiple times to verify the repeatability of the fabrication process and their boiling heat transfer performance. Hydrophobic or superhydrophobic surfaces have the HPO prefix, and hydrophilic or superhydrophilic surfaces have the HPI prefix. Laser-textured surfaces were prepared either using a variable or an equidistant scanning separation (denoted as VS and ES, respectively) to produce microcavities or were fully textured (FT) without the aim of producing microcavities. A detailed description of the naming convention can be found in the Experimental Section alongside the fabrication specifics.

SEM images of selected surfaces are shown in Figure 2, while SEM images of all surfaces can be found in Figures S1 to S10. All SEM images were acquired after the surface has been exposed to boiling. The microstructure of FT surfaces is aligned along the traces of parallel laser beam passes (vertically as shown in Figure 2a), and while the surface exhibits some porosity, there are no distinct cavities on the surface, which could trap vapor and serve as preferential nucleation sites. VS and ES surfaces, on the other hand, show the presence of an abundance of microcavities on top of laser-induced ridges (Figure 2b,c), which form between two parallel consecutive laser beam passes across the surface. These microcavities are shown in detail at a higher magnification in Figure 2d. There is no evident difference between the SEM images of HPO and HPI surfaces fabricated using the same laser texturing parameters as the CVD-fabricated (super)hydrophobic HTMS coating is only a few nanometers thick.[34]

Cross sections of a HPO FT and a HPI VS surface were made using focused ion beam (FIB) milling and are shown alongside the results of the energy-dispersive X-ray spectroscopy (EDS) 2D mapping of O and Al elements in Figure 2e,f, respectively. The oxide layer is only a few hundred nanometers thick on both surfaces and can also be observed in EDS images as a region of increased oxygen concentration (yellow color in the 2D EDS maps denotes a higher concentration of the analyzed element). Additional FIB cross-section images and EDS analyses of different areas can be found in Figures S11 and S12 and S13 to S16 in Section S2, respectively. The porosity of the oxide layer and the expected temperature drop across it due to its thermal resistance is analyzed in Section S3 (Figure S13). Based on the observed thickness and estimated effective thermal conductivity, the temperature drop across the oxide layer is estimated to be less than 0.2 K at 1.5 MW m^{-2} (see Section S3M).

The average density of microcavities on various VS or ES surfaces is between 650 and 950 cavities/mm^2 and was determined by identifying microcavities on selected SEM images at 500× magnification. Microcavities were treated as ellipses, and their mean diameter was determined from the lengths of the semiminor and semimajor axes. The average mean cavity diameters on VS and ES surfaces were 2.8 and 4.2 μm, respectively. An analysis of cavity mean diameter distribution for VS and ES surfaces is shown in Figure 3a. It is evident that, while a similar percentage of microcavities with mean diameters between 1 and 5 μm are present on both VS and ES surfaces, the latter have a significantly higher number of larger cavities (>5 μm) and VS surfaces have a larger percentage of smaller cavities with diameters below or equal to 1 μm. This is a direct result of the texturing strategy as the VS surfaces have the potential to host microcavities in a broader range of dimensions due to the use of several different scanning line separations (between 55 and 65 μm) where a different overlap of the resolidified material can result in varying levels of surface porosity. As the ES surfaces were textured using only the 65 μm scanning line separation, larger cavities are expected to appear than with using a smaller spacing of 55 μm (see Section S5, Figure S19), which in turn causes the distribution of the mean cavity diameters to be skewed toward larger values. This was further confirmed through the analysis of low magnification SEM images where microcavities were measured and counted on VS surfaces on (i) scanning lines up to 55 μm apart and (ii) scanning lines more than 60 μm apart and on ES surfaces with results shown in Figure 3b. Due to the lower magnification, the resolution of

https://dx.doi.org/10.1021/acsami.0c01594
ACS Appl. Mater. Interfaces 2020, 12, 24419−24431

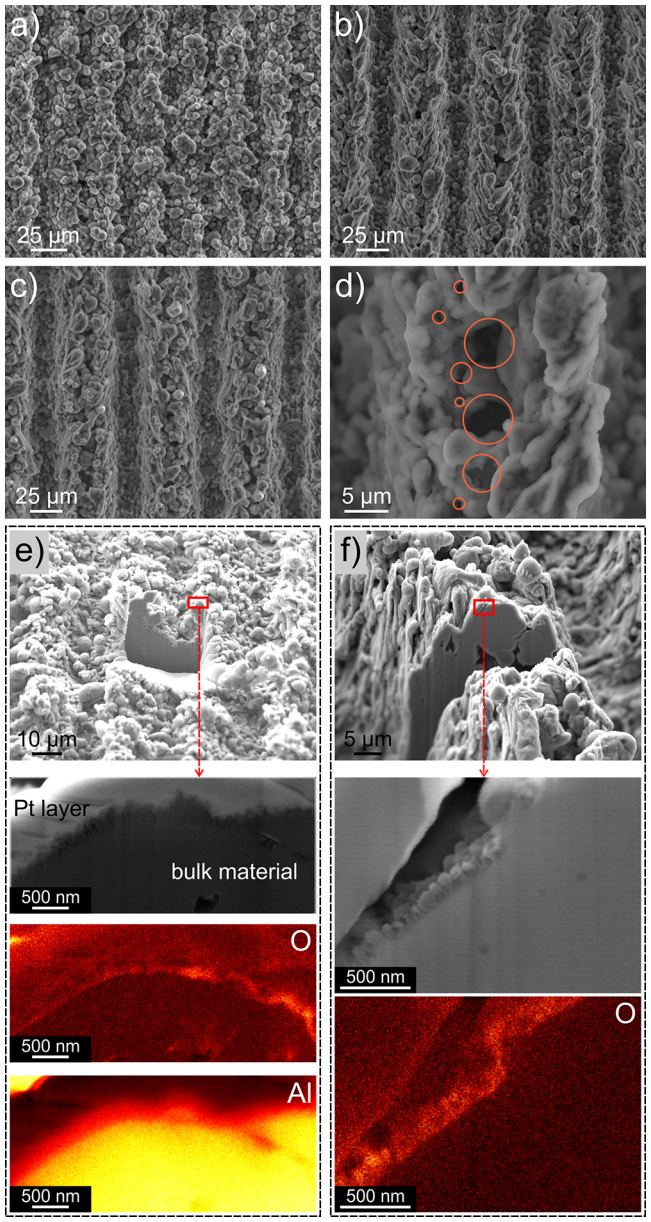

Figure 2. SEM images of surface (a) HPI FT, (b) HPO VS 1, (c) HPO ES 1, and (d) examples of microcavities. (e) FIB cross section and EDS analysis of oxygen and aluminum concentration (the yellow color denotes a higher concentration) on surface HPO FT and (f) HPO VS. Note that FIB-milled surfaces are coated with a 0.5 μm Pt layer to keep the surface layer intact during ion sputtering.

images limits reliable identification of microcavities to those with a diameter of at least 1 μm. Furthermore, the top-down view of SEM images might obscure the identification of some microcavities on the side of the resolidified ridge. Figure 3b clearly shows that lower scanning line separation results in a higher percentage of smaller microcavities (<5 μm), which contributes to the overall shift of the microcavity diameter distribution toward lower values on VS surfaces compared to ES surfaces, as shown in Figure 3a. The analysis of low magnification SEM images also showed that the density of microcavities is lower on scanning lines closer together (approximately 500 microcavities/mm^2 for separations under 55 μm and up to 1000 microcavities/mm^2 for separations above 60 μm), although smaller spacing results in overall smaller cavities, many of which might not have been detected. Low magnification SEM images for separations under 55 μm and above 60 μm are shown in Section S5 in Figure S20a,b, respectively.

Due to a scanning head resolution of 2 μm, the spacing of the laser scanning lines might deviate slightly from the predicted value. This further justifies the use of variable separation to ensure that microcavities form at least for some of the used separations even when using a low-cost scanner with limited spatial resolution.[23]

The apparent contact angle of all surfaces recorded before and after boiling had taken place on them is listed in Table 1. Applying the HTMS coating to a smooth surface produces a hydrophobic surface that does not exhibit a roll-off angle (surface HPO smooth). For true superhydrophobicity and existence of a roll-off angle, micro- and nanoscale surface roughnesses are required.[35−37] The latter can be easily achieved with laser texturing since melting, ablation, and subsequent solidification of the material will induce micro-roughness, while oxide growth will cause the appearance of nanostructures. Laser-textured and subsequently CVD-coated surfaces exhibited an apparent static contact angle above 150° and a roll-off angle below 5°, which is in accordance with the literature.[25,38−41] The dynamic contact angles were measured on selected superhydrophobic surfaces to aid discussion regarding the heat transfer enhancement. Surfaces HPO FT, HPO ES, and HPO VS exhibited the following contact angle hysteresis (CAH): 3.7 ± 2.2°, 4.6 ± 2.9°, and 4.7 ± 2.6°, respectively. Dynamic contact angles are listed in Section S6 (Table S2). Judging from these results, the contact angle hysteresis is not significant and the surfaces cannot be described as parahydrophobic.

Exposure to an aqueous environment will slightly diminish the contact angle since most silane coatings are susceptible to hydrolysis without oxane bond reformation, leading to coating failure with time.[42,43] Several hours of exposure to saturated water universally reduced the contact angle on HPO surfaces, although all surfaces (with the exception of HPO smooth) still exhibited hydrophobicity after boiling experiments. The roll-off angle disappeared post-boiling on some HTMS-coated surfaces and remained lower than 5° on the rest, indicating inconsistent degradation that should be investigated in the future. Exposure to water also modifies the wettability of hydrophilic surfaces, which transition from the initial superhydrophilicity in the saturated Wenzel regime (caused by an abundance of high surface energy oxides present on the surface directly after laser texturing) toward hydrophilicity with a nonuniform droplet spreading due to directional (anisotropic) surface morphology.[24] Such nonuniform wettability has been observed previously on laser-textured surfaces.[28,44,45] The change in contact angle can be explained by pseudoboehmite ($Al_2O_3 \times xH_2O$, $1 \leq x \leq 2$) and bayerite ($Al(OH)_3$) growth on aluminum surfaces during exposure to water at elevated temperatures since the transition of their surface chemistry also alters their free surface energy and wettability.[46−48]

2.2. Pool Boiling Performance. Boiling performance of all surfaces was evaluated using saturated water at atmospheric pressure and recorded in the form of boiling curves showing the relationship between the surface superheat (i.e., the temperature difference between the surface and the water) and the heat flux. To ensure efficient operation of systems utilizing boiling heat transfer, it is desirable for the surface superheat to be low and the boiling curve to be as steep as

https://dx.doi.org/10.1021/acsami.0c01594
ACS Appl. Mater. Interfaces 2020, 12, 24419−24431

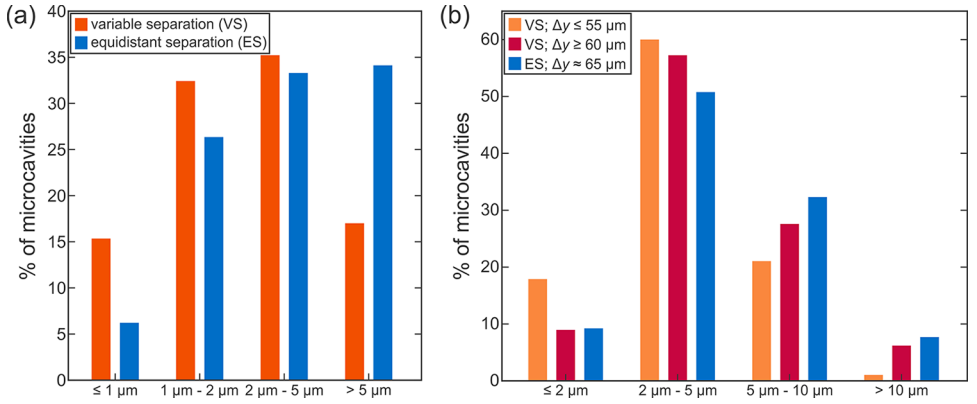

Figure 3. (a) Distribution of microcavity mean diameters on VS and ES surfaces obtained through the analysis of high magnification SEM images and (b) distribution of microcavity mean diameters on laser-induced ridges, generated by a specific scanning line separation on VS and ES surfaces observed on low magnification SEM images.

possible, which translates into high heat transfer coefficients quantifying the heat transfer performance. Furthermore, the transition from natural convection into nucleate boiling (i.e., the onset of nucleate boiling) should ideally also occur at a low surface superheat. Boiling curves were recorded up to the critical heat flux incipience with multiple repetitions of each measurement.

Figure 4a shows a comparison of boiling curves for surfaces without microcavities, which serve as a baseline to which the enhancements are compared to. It is evident that the superhydrophilic, fully laser-textured surface (HPI FT) does not significantly enhance the boiling process since its boiling curve roughly coincides with that of the reference (untreated) surface. The CHF is enhanced by 21%, which is caused by the (super)hydrophilic nature and porosity of the surface, enabling better and more rapid rewetting of the surface after the departure of individual bubbles and thus preventing local surface dryouts. This agrees with the established literature reporting higher CHF values on (super)hydrophilic and/or porous surfaces without a major heat transfer coefficient enhancement.[13−15,49,50] The same surface, but coated with HTMS (HPO FT), will exhibit superhydrophobicity. However, the surface does not become fully covered by a vapor film soon after the boiling incipience and a CHF comparable to that of the untreated sample is observed. The heat transfer coefficient is enhanced up to 290% at low heat fluxes and by 120% at CHF in comparison with the reference. Finally, a smooth surface coated with HTMS (HPO smooth) will be hydrophobic rather than superhydrophobic with no roll-off angle and it will offer a small enhancement over the reference surface in terms of the heat transfer coefficient and a minor CHF increase. This could be attributed to easier penetration of water to the surface microstructure in comparison with the superhydrophobic HPO FT surface, which prevents the early formation of a vapor film. Since the adhesion of the coating is poor on smooth surfaces, degradation is observed post-boiling with a contact angle below 90°.

Boiling performances of superhydrophilic and superhydrophobic microcavity surfaces are shown in Figure 4b. Both HPO VS and HPO ES surfaces exhibit extreme boiling performance with enhancements of the heat transfer coefficient of several hundred percent and an increase in CHF values of up to 41% in comparison with the reference surface. The remarkable heat transfer performance of superhydrophobic microcavity surfaces, which departs from the usual observations during boiling on superhydrophobic surfaces and was also exhibited by the HPO FT surface to a certain extent, can be explained by the penetration of water to the surface and the appearance of the Wenzel wetting regime despite the apparent superhydrophobicity of the surface, as suggested by Allred et al.[18] Proper degassing of the surfaces was confirmed through additional tests shown in Figure S29. Boiling performance of improperly degassed surface in the initial Cassie−Baxter wetting state is significantly different to that of the properly degassed surface in the initial Wenzel wetting state, which also agrees with the results of Allred et al.[18]

The HPO ES 1 surface performs better at low heat fluxes (up to 200 kW m^{-2}) where it transitions into nucleate boiling at a lower surface superheat and exhibits higher heat transfer coefficients. This can be explained by the fact that ES surfaces have a greater percentage of larger microcavities from which bubbles can grow at lower superheats, which can be deduced from the following expression by combining the bubble Laplace pressure and accounting for the Clausius−Clapeyron relation[51,52]

$$T_w - T_{sat} = \frac{2\sigma T_{sat}}{h_{fg}\rho_g r} \tag{1}$$

Here, T_w denotes the boiling surface temperature (wall temperature), T_{sat} is the saturation temperature, σ is the surface tension, h_{fg} is the latent heat of vaporization, ρ_g is the vapor density, and r is the radius of the bubble embryo, which equals to cavity radius in the situation when the cavity is completely filled with vapor (see Section S7 for a detailed explanation). Similarly, a more complex analysis is possible by accounting for factors like the surface wettability in accordance with nucleation criteria such as Hsu's criterion[53]

$$\{r_{min}, r_{max}\} = \frac{\delta \sin\theta}{2(1+\cos\theta)}\left(1 \mp \sqrt{1 - \frac{\sigma T_{sat}(1+\cos\theta)}{h_{fg}\rho_g \delta (T_w - T_{sat})}}\right) \tag{2}$$

where θ is the contact angle, δ is the thermal boundary layer thickness, and r_{min} and r_{max} are the minimal and maximal cavity radii suitable for nucleation, respectively. In both equations the temperature difference (surface superheat) required for the nucleation to occur is inversely related to the cavity diameter; the larger the cavity, the lower the required superheat.

https://dx.doi.org/10.1021/acsami.0c01594
ACS Appl. Mater. Interfaces 2020, 12, 24419−24431

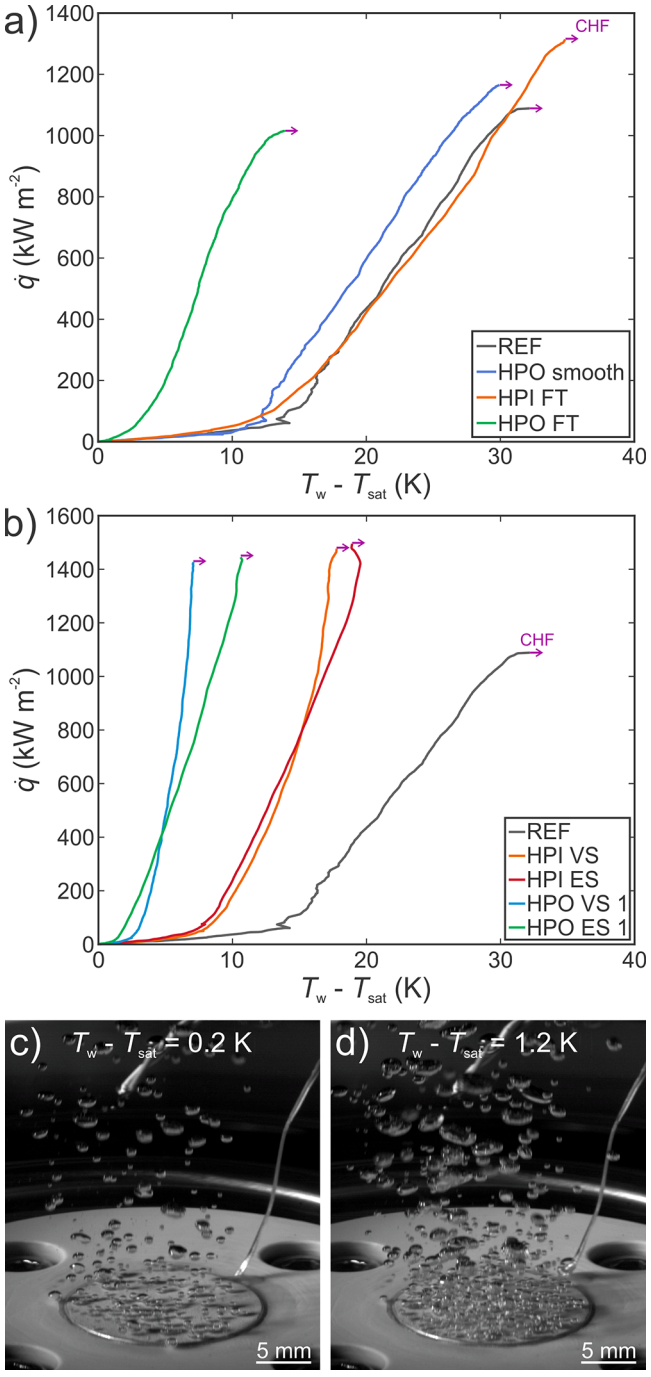

Figure 4. (a) Boiling performance of the reference surface, smooth hydrophobic surface, and fully laser-textured surfaces, (b) boiling performance of superhydrophilic (HPI) and superhydrophobic (HPO) microcavity surfaces, and (c, d) high-speed video snapshots of the boiling process on surface HPO VS 1 at a superheat of (c) 0.2 and (d) 1.2 K.

However, the HPO VS 1 surface demonstrates better performance at high heat fluxes (above 600 kW m^{-2}) with higher heat transfer coefficients up to the CHF incipience. This difference in performance is greater than the measurement uncertainty and can be attributed to a greater percentage of smaller cavities on the VS surfaces and an overall wider range of microcavity diameters with a decreased lower limit of the microcavity diameter range. Additionally, submicrometer microcavities are harder to detect and all of them might not have been successfully identified potentially, increasing their actual density. As the surface superheat increases with increasing heat flux, it follows from eq 1 that smaller microcavities will gradually be activated and start producing bubbles. Moreover, it is evident from eq 2 that an increased surface superheat will broaden the size-range of potentially active microcavities, activating smaller cavities since the largest available will have already been activated at the onset of nucleate boiling. Finally, smaller cavities are more likely to entrap vapor and thus be activated by bubble growth from the already active neighboring sites, ensuring a higher overall number of active nucleation sites on the surface.[54] The same trends are observable on the superhydrophilic microcavity surfaces (HPI VS and HPI ES).

Figure 4c,d shows that nucleation begins at an extremely low superheat on microcavity surfaces and that the number of active nucleation sites is upwards of 25 sites/cm^2, even at only 0.2 K of superheat. Both the surface and water were thoroughly degassed prior to the boiling measurements through vigorous boiling for 60 min to minimize the amount of noncondensable gas entrapment. While some air could inevitably have stayed on the surface and contributed to early nucleation, the surfaces were further degassed during the boiling experiments where the leftover vapor replaces the entrapped air. Additionally, during the CHF incipience at the end of each experimental run, the entire surface became covered by a vapor film, further promoting displacement of air and replacement by vapor. Afterward, the surface was cooled together with the surrounding water to below 90 °C, ensuring the collapse of vapor nuclei before proceeding with the next experimental run. Since the pressure inside the cavities is slightly higher due to the curved interface, temperature higher than the saturation temperature at atmospheric pressure is necessary to ensure the existence of entrapped vapor and prevent its collapse, meaning that cooling the surface and water below saturation temperature will effectively collapse the existing vapor nuclei.

Figure 5a shows the results of subsequent experimental runs on several microcavity surfaces. It is evident that the differences between the boiling curves of individual experimental runs are relatively small and in the similar order of magnitude as the measurement uncertainty, which supports the assumption of the negligible effect of possibly entrapped air on an early onset of nucleate boiling.

2.3. Surface Stability and Functionalization Repeatability. The stability of superhydrophobic microcavity surfaces was evaluated through multiple experimental runs with an emphasis on recording possible degradation of boiling performance due to the hydrophobic coating degradation or due to the reduction of the amount of entrapped air. Results in Figure 5a suggest that the degradation of boiling performance is very small and most likely the results of a slight degradation of hydrophobic properties of the HTMS coating, which shifts the boiling curve to the right toward higher superheats and closer to the hydrophilic microcavity surfaces. A further comparison of the boiling curves recorded during repeated boiling runs is shown in Figure S23. Degradation after the first onset of CHF is minimal compared to the degradation experienced by copper surfaces where a modification of surface chemistry and morphology occurs due to the transition between copper oxide forms.[30] Aluminum has the ability to quickly form a stable passive layer, protecting it against further oxidation.[55,56] Overall, the stability is favorable from the

https://dx.doi.org/10.1021/acsami.0c01594
ACS Appl. Mater. Interfaces 2020, 12, 24419−24431

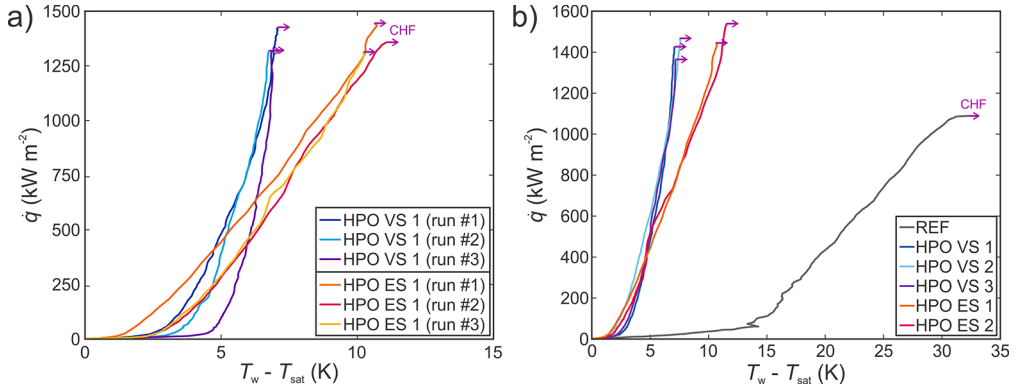

Figure 5. (a) Evaluation of boiling performance stability on HTMS-coated surfaces HPO VS 1 and HPO ES 1. (b) Evaluation of the surface functionalization process repeatability.

applicative standpoint, although evaluation of the long-term stability is still necessary.

Repeatability of the superhydrophobic microcavity surface fabrication process was evaluated by creating two additional HPO VS surfaces (HPO VS 2 and HPO VS 3) and one additional HPO ES surface (HPO ES 2). Boiling performance evaluation of additional surfaces in the form of boiling curves is compared to the performance of the original surfaces in Figure 5b. The boiling curves of each surface type lie closely together (well within the measurement uncertainty), and both the CHF and heat transfer coefficient values are extremely similar, indicating excellent repeatability of the surface functionalization using laser texturing in combination with a superhydrophobic coating application.

2.4. Mechanism of Boiling Performance Enhancement. While both the superhydrophilic fully textured surface (HPI FT) and the superhydrophilic microcavity surfaces (HPI VS and HPI ES) enhanced the critical heat flux, the corresponding superheat was approximately 50% lower on the microcavity surfaces (see Section S8 and the comparison of all boiling curves in Figure S22). This clearly shows that boiling performance enhancement arises due to microcavities. Moreover, it indicates that a fully textured surface without specifically engineered features (i.e., microcavities) does not enhance the boiling performance by much, despite its superhydrophilicity. According to our previous study,[28] the nucleation site density is 20−40 times higher on surfaces partially covered by microcavities compared to an untreated surface and the nucleation frequency is increased 2-fold. Furthermore, the bubble contact and departure diameters are much smaller on the microcavity surface. Considering the findings by Preckshot and Denny,[57] who report that the diameters of detached bubbles decrease with increasing nucleation site density, this explains the reduced horizontal bubble coalescence and thus delayed dryout due to vapor blanketing. Based on the established understanding of the effect that superhydrophilic surfaces have on the boiling performance, the superheats on the HPI VS and HPI ES surfaces would be much higher if the microcavities did not serve as preferential nucleation sites circumventing the disadvantageous high energy barrier for nucleation on "plain" superhydrophilic surfaces.

Similar differences can be observed when comparing the performance of the superhydrophobic surfaces, which exhibit nearly identical dynamic contact angles with a low contact angle hysteresis and are, therefore, not parahydrophobic.[11] Since boiling is initiated from the Wenzel wetting regime, the HPO FT surface exhibits favorable boiling performance with the heat transfer coefficient reaching 80 kW m^{-2} K^{-1}, although its performance is significantly lower than that of hydrophobized microcavity surfaces. This happens since microcavities are able to initiate boiling at an even lower superheat and provide an abundance of (potentially) active nucleation sites that enhance the boiling performance at low and medium heat fluxes and increase the CHF. The final definitive evidence showing that the microcavities are responsible for different boiling performance of HPO FT/VS/ES surfaces despite the same wetting behavior comes from different microcavity sizes and size distributions on HPO ES and VS surfaces (Figure 3). The ES surface contains larger microcavities from which nucleation starts at lower superheats. However, while the microcavity size distribution is limited on the HPO ES surfaces, HPO VS surfaces exhibit superior behavior at higher heat fluxes where smaller microcavities are activated. The fabrication and comparison of three VS and two ES superhydrophobic surfaces (Figure 5b) proves that this trend is not just a one-time anomaly.

To summarize, a comparison of both superhydrophilic and superhydrophobic microcavity surfaces with corresponding fully treated surfaces shows that microcavity surfaces always exhibit superior performance when the wettability of the surfaces is similar. Differences in boiling performance of ES and VS surfaces due to different microcavity size distributions further prove that an abundance of microcavities serving as active nucleation sites is the answer to enhanced boiling performance. The superhydrophobic coating helps initiate nucleation at lower surface superheats and reduce the value of the latter parameter throughout the nucleate boiling range due to favorable vapor entrapment behavior.

While both HPI and HPO microcavity surfaces shown in Figure 4b offer improved heat transfer performance and a similar increase of the CHF, the heat transfer coefficient enhancement is much greater with hydrophobic surfaces, which enable the onset of nucleate boiling to occur at a lower surface superheat.[58,59] A comparison of the heat transfer coefficients is shown in absolute terms in Figure 6a and relative to the reference surface at four distinct heat fluxes in Figure 6b. The highest heat transfer coefficient on a superhydrophilic microcavity surfaces was recorded at CHF on surface HPI VS (83.1 kW m^{-2} K^{-1}), which marks a 146% enhancement over the reference surface. The superhydrophobic microcavity surface with a variable scanning separation HPO VS 1, on

https://dx.doi.org/10.1021/acsami.0c01594
ACS Appl. Mater. Interfaces 2020, 12, 24419−24431

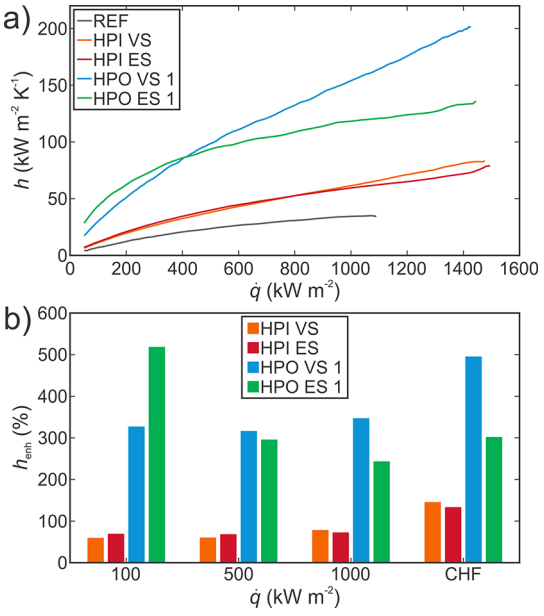

Figure 6. (a) Boiling performance of best-performing surfaces displayed as the heat transfer coefficients versus the heat flux and (b) as a comparison of the heat transfer coefficient enhancement relative to the reference surface.

the other hand, exhibits 2.4× higher heat transfer coefficient (201.4 kW m^{-2} K^{-1}), which represents a 496% enhancement over the reference surface at their respective CHF point. While most enhanced surfaces found in the literature including our HPI surfaces offer heat transfer enhancement especially at high heat fluxes, HPO microcavity surfaces offer enhancements of up to 519% even at a low heat flux of 100 kW m^{-2} (7% of the CHF on the respective surface).

The extreme boiling performance enhancement offered by the superhydrophobic microcavity surfaces is further graphically explained in Figure 7 where superhydrophobic and superhydrophilic microcavity surfaces (HPO μC and HPI μC, respectively) are compared with an untreated reference surface (REF) at three distinct heat fluxes. An idealized cross section of each surface is shown together with a temperature scale on the left. The actual temperatures are arbitrary, and the departed bubbles are not drawn to scale. At a very low heat flux, the superhydrophobic microcavity surface will already have entered the nucleate boiling regime due to the lower energy barrier for the formation of the vaporous phase on surfaces with a low wettability.[60] At the same heat flux, the superhydrophilic microcavity and the untreated surfaces have not yet formed an entrapped vapor nucleus and the entire heat flux is removed only by natural convection. Since the heat transfer coefficient of nucleate boiling is much higher than that of the natural convection, an enhancement of up to 330% is present on the superhydrophobic microcavity surface. At the slightly higher heat flux, both microcavity surfaces will have entered the nucleate boiling regime associated with high heat removal rates, while the reference surface still has not formed a vapor nucleus and transitioned into nucleate boiling. The latter is mostly due to the absence of cavities with suitable dimensions for nucleation at the given surface superheat. In general, only steep and poorly wetted cavities have been shown to entrap gas.[61] Similarly, Qi et al.[62] observed that only deep cavities are suitable for trapping vapor, and while such cavities are unlikely to form during sanding/polishing, they are clearly present on the microcavity surfaces. Interconnected cavities, which form using laser texturing, further increase the possibility of vapor entrapment.[23] At such a heat flux level, an enhancement upwards of 70 and 600% is possible with superhydrophilic and superhydrophobic microcavity surfaces, respectively. Finally, all three surfaces are in the nucleate boiling regime at the third and highest heat flux where the relative heat transfer coefficient enhancement is not as extreme as before since the same mechanism of heat removal is present on all three compared surfaces.

The results demonstrate that, while the establishment of the Wenzel regime will increase the heat transfer coefficient, CHF will not be increased significantly. The superhydrophobic HPO FT surface without suitable microscopic topographical features for boiling enhancement notably increases the heat transfer coefficient, but the CHF is comparable to that of the reference surface. A significant CHF increase is achieved only when the Wenzel regime is combined with a suitable microstructure, which enables effective nucleation throughout the nucleate boiling regime. This is clearly demonstrated on superhydrophobic microcavity surfaces (HPO VS and HPO ES).

The presented results confirm the findings of Allred et al.,[18] who showed that efficient boiling heat transfer is possible on superhydrophobic surfaces if the initial Wenzel wetting regime is achieved. However, the latter authors recorded a CHF

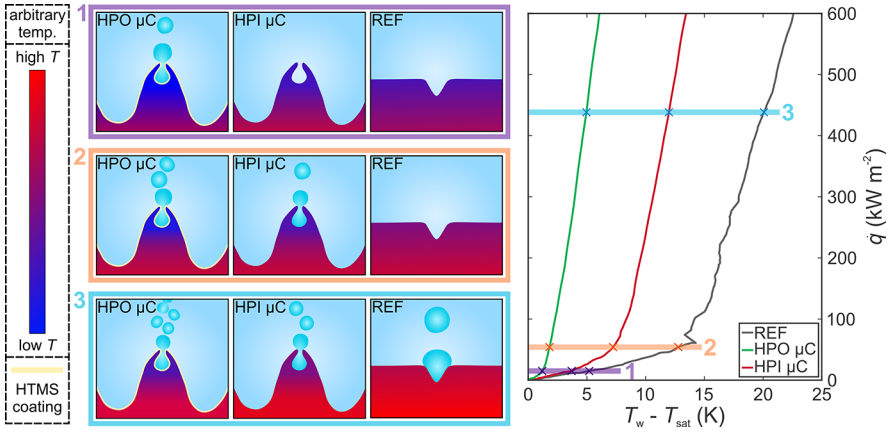

Figure 7. Schematic depiction of the nucleation process enhancement with microcavities (μC) and superhydrophobic HTMS coating at three distinct heat fluxes. Microcavities and bubbles are not drawn to scale.

https://dx.doi.org/10.1021/acsami.0c01594
ACS Appl. Mater. Interfaces 2020, 12, 24419−24431

Table 2. Comparison of Pool Boiling Performance of Previously Reported Laser-Textured Surfaces against Superhydrophobic Microcavity Surfaces Presented in this Study

authors	material	laser pulses	CHF (kW m^{-2})	ΔCHF (%)	h (kW m^{-2} K^{-1})	Δh (%)
Kruse et al.[26]	stainless steel	fs	1420	+56	67.4	+193
Kruse et al.[64]	copper	fs	1300[a]	−22	70.3[a]	+1
Kruse et al.[65]	copper	fs	1430	−15	87.0	+24
Nirgude and Sahu[27]	copper	ns	N/A[b]	N/A	41.5[b]	+80
Zupančič et al.[28]	stainless steel	ns	N/A[b]	N/A	35.4[b]	+177
Voglar et al.[29]	stainless steel	ns	1200[c]	+269	48.2[c]	+166
Može et al.[30]	copper	ns	1580	+89	76.1	+129
Mani et al.[66]	copper	ps	2260	+103	97.5	+153
this study	aluminum	ns	1539	+41	201.4	+496

[a]Only surfaces without microchannels are considered. [b]CHF not measured, HTC at the highest heat flux measured on an individual surface. [c]Thin heater burnout.

similar to that of the reference surface. Using superhydrophobic microcavity surfaces, we not only doubled the heat transfer coefficient achieved by Allred et al. but also enhanced the CHF by a significant margin. Microcavities in the appropriate size range for the nucleation under given boiling conditions provide an abundance of nucleation sites enabling efficient bubble formation, whereas the superhydrophobic coating reduces the activation temperature for bubble formation and growth. Furthermore, the Wenzel wetting regime limits the spreading of the vapor film along the surface and limits horizontal coalescence, thus preventing local dryouts and hotspots. Our findings allude to the fact that superhydrophobicity as such does not exist under present boiling conditions on surfaces where the low surface energy coating is coupled with surface microstructuring, and the heat transfer enhancement in light of a low superheat nucleate boiling onset can be explained by a lowered energy barrier for nucleation because of the coating's low surface energy and not because of air entrapment, which otherwise lowers surface superheat at the nucleate boiling onset and significantly changes the nucleation and bubble dynamics.[61,63]

2.5. Enhancement Magnitude Evaluation. The performance of newly developed hydrophobized laser-textured aluminum surfaces is compared to the previously reported pool boiling enhancements achieved using laser-textured surfaces in Table 2. Most research studies were performed on copper and stainless steel, while no references dealing with boiling heat transfer on laser-textured aluminum could be found. All studies shown in Table 2 were conducted using water. Authors of the reviewed publications utilized either nanosecond (ns), picosecond (ps), or femtosecond (fs) laser pulses for surface texturing. As the highest achieved critical heat flux (CHF) and the highest heat transfer coefficient (h) were often not recorded on the same enhanced surface, highest reported values were used regardless of the surface (e.g., in the present study, the highest CHF was achieved on the surface HPO ES 2 and the highest heat transfer coefficient was achieved on the surface HPO VS 1). Furthermore, CHF was not recorded during some of the experiments due to the limitations of the experimental setup or if the measurements were performed on thin foils where the CHF was either (i) not recorded to avoid heater burnout or (ii) the burnout heat flux was recorded, but due to the low thermal effusivity of the heater, the realistic CHF could be higher.

The results in Table 2 clearly show that the highest heat transfer coefficients recorded during this study are at least 2 times higher than the next highest reported value. Furthermore, the heat transfer enhancement of almost 500% on hydrophobized microcavity surfaces clearly outmatches all other laser-textured surfaces for which the highest enhancement does not exceed 200%. Additionally, the heat transfer coefficient enhancement is often achieved either only at high heat fluxes and/or high surface superheats. This diminishes the practical value of such enhanced surfaces as most applications in (micro)electronics require low superheats of the cooling (boiling) surface. While both the absolute CHF value and the CHF enhancement are not the highest reported, their values are still respectable, especially considering (i) the extreme value of the heat transfer coefficient achieved at the same time and (ii) that the possibility of efficient boiling on superhydrophobic surfaces is a new concept in boiling heat transfer enhancement.

The surfaces presented in this paper are capable of achieving a heat transfer coefficient of 201 kW m^{-2} K^{-1} at a superheat of only 7.1 K, making them very suitable for sensitive cooling applications where the low temperature of the cooled component is required together with a high heat removal rate. For example, if the developed surfaces were used to cool an electronic component dissipating a heat flux of 100 kW m^{-2} (approximate surface-averaged heat flux on the most powerful modern consumer desktop central processor units), then the HPO ES 1 surface would be able to provide a surface superheat of just 2.3 K in comparison with a superheat of 14.3 K for the untreated reference surface due to the much higher heat transfer coefficient at a low heat flux (44 kW m^{-2} K^{-1} versus 7 kW m^{-2} K^{-1}, respectively). Another important advantage of the proposed fabrication method is the straightforward and scalable approach with reasonably low costs and provisions for rapid production.

3. CONCLUSIONS

In summary, we demonstrate extreme boiling performance of superhydrophobic microcavity surfaces fabricated by combining direct laser texturing and chemical vapor deposition of a hydrophobic silane. Both superhydrophilic and superhydrophobic surfaces with laser-engineered microcavities exhibit significantly enhanced boiling heat transfer with favorable repeatability of the surface functionalization technique. The highest achieved heat transfer coefficients exceed 200 kW m^{-2} K^{-1} on a superhydrophobic microcavity surface, marking a five-time enhancement at a low superheat of 7.1 K. The superhydrophobic nature of the functionalized surfaces does not necessarily cause adverse boiling performance, confirming that the Wenzel wetting regime is possible during boiling on

https://dx.doi.org/10.1021/acsami.0c01594
ACS Appl. Mater. Interfaces 2020, 12, 24419−24431

apparently superhydrophobic surfaces. By combining laser-induced microcavities with a superhydrophobic coating, we demonstrate a significantly increased CHF, proving that enhanced boiling heat transfer is possible on superhydrophobic surfaces with an appropriate microstructure where the establishment of the Wenzel wetting regime is achieved. With this, we also demonstrate that both the wettability of the surface and its topography are important factors influencing the boiling performance in a complementary manner. The fabrication process has great potential for the development of a new generation of heat transfer surfaces for enhanced phase change as it can be used to quickly and repeatably produce low-cost, high-performance phase-change heat transfer surfaces.

4. EXPERIMENTAL SECTION

4.1. Nanosecond Laser Surface Texturing. Samples were laser-textured using a nanosecond fiber laser (SPI Lasers, G4, SP-020PA-HS-S-A-Y) with a wavelength of λ = 1060 nm, a beam quality of M^2 = 1.3, and a pulse duration of 45 ns at full width at half-maximum (FWHM). The laser beam was guided across the surface of the sample using an F-Theta lens (focal distance f_L = 163 mm) and a scanning head (Raylase, SS-IIE-10) with an angular resolution of 12 μrad (which equals to 2 μm at f_L = 163 mm). The beam spot diameter equaled to 38 μm and the samples were textured in the focal plane. Surfaces with cavities (VS and ES) were treated using an average power of laser pulses of 17.8 W, a peak pulse fluence of 17.3 J cm^{-2}, a pulse repetition rate of 180 kHz, and a scanning velocity of 400 mm s^{-1}. Fully textured (FT) surfaces were treated with an average power of 7.4 W, a peak pulse fluence of 14.4 J cm^{-2}, a pulse repetition rate of 90 kHz, and a scanning velocity of 300 mm s^{-1}. The threshold fluence for laser ablation of the used material (F_{th}) was evaluated by drilling linear microchannels using different peak fluences (average laser powers), as previously described by Gregorčič et al.[32] In this way, a value of $F_{th} \approx 3$ J cm^{-2} was determined for a 6082 aluminum alloy with the same surface finish as used during the laser functionalization of boiling surfaces. The samples were textured with parallel laser beam passes (0° texturing). A constant scanning line separation of Δy = 65 μm was used for surfaces with microcavities produced by an equidistant separation value (ES), while fully textured surfaces (FT) were obtained at Δy = 30 μm. Surfaces with microcavities and a variable separation (VS) were textured using a variable separation of Δy = {55, 60, and 65 μm} to increase the size range of the produced cavities (see Section S4 for the concept of variable separation). All samples were textured in air atmosphere with no forced air movement. All surfaces exhibited superhydrophilicity immediately after laser texturing; they were in a saturated Wenzel regime with a contact angle of 0°.[24] If no subsequent treatment was applied to the surface, then it was denoted as a hydrophilic surface (HPI). An untreated, finely sanded aluminum surface was used as a reference to compare all results to and denoted as REF.

4.2. HTMS Coating Fabrication. Selected surfaces were hydrophobized using the chemical vapor deposition (CVD) process.[34,43] The coating mixture was prepared by mixing 0.05 mL of (heptadecafluoro-1,1,2,2-tetrahydrodecyl)trimethoxysilane (abbreviated to HTMS; Gelest Inc.) with 0.95 mL of toluene (≥99.7%, Honeywell International Inc.) in a glass vial at room temperature. The vial was then placed in a 1000 mL plastic container together with the samples and covered by aluminum foil. The plastic container was placed in a preheated oven at 85 °C for 90 min at atmospheric pressure for the coating to form. After 90 min, the oven was turned off and the plastic container was allowed to cool down in the oven before it was taken out and the samples were removed. Having undergone the HTMS treatment, the surfaces were denoted as hydrophobic surfaces (HPO).

4.3. Surface Morphology Analysis. The morphology of samples was analyzed using a scanning electron microscope (JEOL JSM-6500F) at an accelerating voltage of 15 kV utilizing a secondary electron detector. SEM images were used to analyze the diameters of cavities on laser-textured surfaces. Since most cavities are elliptical, the semimajor (r_{ma}) and semiminor (r_{mi}) axes were measured and the mean radius (r_μ) was calculated to be $(2r_{ma} + r_{mi})/3$. The surface density of cavities was calculated by manually counting all recognizable cavities on SEM images and dividing their count by the surface area depicted in the given SEM image. Cross sections were fabricated by focused ion beam (FIB) milling (Zeiss CrossBeam 550 FIB/SEM dual beam microscope), and their SEM images were taken at a sample tilt angle of 54°. Prior to FIB milling, the surfaces were protected by deposition of a 0.5 μm thick layer of Pt. The 2D mapping of elemental composition of the cross sections was performed by the Octane Elite EDS system (produced by EDAX) using the TEAM software.

4.4. Contact Angle Measurement. The apparent contact angle (CA) was measured at room temperature and atmospheric pressure using twice-distilled water and a custom contact angle goniometer utilizing an IDS UI-3060CP high-speed camera with a macro lens. On every surface, five measurements were conducted by depositing 15–20 μL of droplets onto different parts of the surface and the captured images were processed using a custom MathWorks MATLAB script to obtain the average value of the contact angle. Measurements were performed both before and after the boiling performance measurements. While some authors[67] denounce the importance of (static) CA as it can take any value between the advancing and receding CA, we believe that calculating the apparent CA as the arithmetic mean of multiple (static) CA measurements provides grounds for comparison of surfaces and correlation of their wetting properties with boiling behavior. The advancing and receding contact angles were measured using the same goniometer and the droplet inflation/deflation method. A recorded high-speed footage was analyzed to obtain relevant images of the triple contact line movement and the values of the dynamic contact angles.

4.5. Pool Boiling Performance Measurement. Pool boiling performance was evaluated using a custom experimental setup previously described in ref.[30] and shown schematically in Section S10. Circular 6082 aluminum alloy samples (AlCu d.o.o.) with a thickness of 4 mm and diameter of 18 mm were utilized for boiling experiments. A 9 mm long, 1 mm diameter hole was drilled into the middle of the side of the sample into which a thin type K thermocouple (Class 1 wire, 5TC series; Omega Engineering Inc.) was embedded. Samples were mounted into a low thermal conductivity polymer (PEEK) holder using a silicone O-ring, and the gap was sealed with flexible epoxy resin (Duralco 4538; Cotronics Corp.). The boiling chamber was constructed from a glass cylinder (internal diameter of 100 mm) between two stainless steel flanges and was filled with approximately 500 mL of coolant during the measurements. The holder with the sample was attached to the bottom flange so that the boiling process took place only on top of the sample's flat horizontal surface. Heat was supplied to the sample using a copper heating block and three 400 W, AC-powered cartridge heaters, whose power was regulated with a variable transformer. Thermal paste (MX-4; Arctic GmbH) was used between the sample and the heating block to ensure a low thermal resistance of less than 0.15 K W^{-1}. The spatial temperature gradient along the axis of the heating block was measured by four type K thermocouples, 5 mm apart from one another. Twice-distilled water (3478.2; Carl Roth GmbH) at atmospheric pressure and in a saturated state was used as the coolant and was degassed though vigorous boiling using an immersion heater for 60 min prior to any measurements. The vapor was condensed in a glass reflux condenser and returned to the boiling chamber. A detailed depiction of the experimental setup is shown in Figures S24 to S26. Measurements were repeated multiple times on every surface to evaluate their stability. During each measurement, the power of cartridge heaters was slowly increased so that the heat transfer performance of the tested surface was measured from zero to the incipience of the CHF. The heat flux was increased by a rate of less than 2 kW m^{-2} s^{-1} (see Section S11 where the dynamic measurement approach is validated). Data was collected at a rate of 1 Hz using a data logger (34970A; Keysight Technologies) and a 16-

https://dx.doi.org/10.1021/acsami.0c01594
ACS Appl. Mater. Interfaces 2020, 12, 24419−24431

channel multiplexer module (34902A; Keysight Technologies). A moving average filter was used to reduce the effect of thermocouple noise in data processing.

4.6. Data Reduction and Measurement Uncertainty. Heat flux was calculated using Fourier's law of steady-state heat conduction based on the temperature measurements along the heater block and the temperature-dependent value of the copper block's thermal conductivity.[68] The calculated heat flux value was used together with the temperature inside the sample and the temperature-dependent thermal conductivity of aluminum to extrapolate the temperature of the surface. Superheat of the surface was calculated from the temperature of the surface and the average temperature of the water, measured by two submerged type K thermocouples. Finally, the heat transfer coefficient was calculated by dividing the heat flux and the corresponding surface superheat. A detailed description of data reduction including relevant equations can be found in Section S13. The heat flux measurement uncertainties were 10.5 and 53 kW m^{-2} at 100 kW m^{-2} and 1 MW m^{-2}, respectively. The surface superheat measurement uncertainties were 0.38 and 1.07 K at 100 kW m^{-2} and 1 MW m^{-2}, respectively. The uncertainty of the heat transfer coefficient depends heavily on the value of both heat flux and surface superheat and therefore varies between surfaces; a worst-case value at a heat flux of 500 kW m^{-2} is 12.0 kW m^{-2} K^{-1}.

■ ASSOCIATED CONTENT

Supporting Information

The Supporting Information is available free of charge at https://pubs.acs.org/doi/10.1021/acsami.0c01594.

Additional SEM images of the fabricated surfaces; FIB, SEM, and EDS analysis of the oxide layer; estimation of the temperature drop across the oxide layer; description of the laser texturing strategy; effect of scanning separation on microcavity formation; dynamic contact angle measurements; explanation of gas entrapment in surface cavities; comparison of boiling performance of all surfaces; evaluation of surface stability under repeated boiling tests; detailed description of the experimental setup for boiling performance evaluation; validation of the dynamic measurement approach; effect of fluid degassing on boiling behavior; and data reduction procedure and measurement uncertainty calculations (PDF)

■ AUTHOR INFORMATION

Corresponding Authors

Matic Može − *Faculty of Mechanical Engineering, University of Ljubljana, 1000 Ljubljana, Slovenia;* orcid.org/0000-0002-6569-4037; Email: matic.moze@fs.uni-lj.si

Matevž Zupančič − *Faculty of Mechanical Engineering, University of Ljubljana, 1000 Ljubljana, Slovenia;* Email: matevz.zupancic@fs.uni-lj.si

Authors

Matej Senegačnik − *Faculty of Mechanical Engineering, University of Ljubljana, 1000 Ljubljana, Slovenia*

Peter Gregorčič − *Faculty of Mechanical Engineering, University of Ljubljana, 1000 Ljubljana, Slovenia;* orcid.org/0000-0003-0459-6369

Matej Hočevar − *Institute of Metals and Technology, 1000 Ljubljana, Slovenia*

Iztok Golobič − *Faculty of Mechanical Engineering, University of Ljubljana, 1000 Ljubljana, Slovenia*

Complete contact information is available at: https://pubs.acs.org/10.1021/acsami.0c01594

Author Contributions

M.M. designed the research, proposed the surface coating, performed the boiling experiments, characterized the surface wettability, and wrote the first draft of the manuscript. P.G. and M.Z. developed the laser texturing method. M.M. and M.S. optimized the laser texturing parameters and prepared the surfaces. M.H. performed the surface characterization. P.G. led the research connected to the surface engineering. M.M, M.Z., and P.G. wrote the final version of the manuscript. I.G. led the research connected to the boiling experiments. All authors have approved the final version of the manuscript.

Funding

This research was funded by the Slovenian Research Agency (P2-0223, P2-0392, P2-0132, J2-1741, and Z2-9215).

Notes

The authors declare no competing financial interest.

■ ACKNOWLEDGMENTS

The authors would like to thank Dr. Barbara Šetina Batič from the Institute of Metals and Technology (Ljubljana, Slovenia) for FIB and EDS measurements. The authors acknowledge the financial support from the Slovenian Research Agency (research core funding nos. P2-0223, P2-0392, and P2-0132 and projects nos. J2-1741 and Z2-9215) and the support of SPI Lasers Ltd. by loan of their fiber laser within the research project "Surface Functionalization by Nanosecond Fiber Laser Texturing (nsFLaT)".

■ ABBREVIATIONS

2D, two-dimensional
CA, contact angle
CAH, contact angle hysteresis
CHF, critical heat flux
CVD, chemical vapor deposition
EDS, energy-dispersive X-ray spectroscopy
ES, equidistant separation
FIB, focused ion beam
FT, fully textured
FWHM, full width at half-maximum
HPO, hydrophobic
HPI,, hydrophilic
HTMS, (heptadecafluoro-1,1,2,2-tetrahydrodecyl)-trimethoxysilane
SEM, scanning electron microscopy
VS, variable separation
μC, microcavity

■ REFERENCES

(1) Alkharabsheh, S.; Fernandes, J.; Gebrehiwot, B.; Agonafer, D.; Ghose, K.; Ortega, A.; Joshi, Y.; Sammakia, B. A Brief Overview of Recent Developments in Thermal Management in Data Centers. *J. Electron. Packag.* **2015**, *137*, No. 040801.

(2) Bar-Cohen, A.; Geisler, K. J. L. Cooling the Electronic Brain. *Mech. Eng.* **2011**, *133*, 38−41.

(3) Song, Z.; Zhang, X.; Eriksson, C. Data Center Energy and Cost Saving Evaluation. *Energy Procedia* **2015**, *75*, 1255−1260.

(4) Trojer, M.; Azizian, R.; Paras, J.; McKrell, T.; Atkhen, K.; Bucci, M.; Buongiorno, J. A Margin Missed: The Effect of Surface Oxidation on CHF Enhancement in IVR Accident Scenarios. *Nucl. Eng. Des.* **2018**, *335*, 140−150.

(5) Andresen, M.; Liserre, M. Impact of Active Thermal Management on Power Electronics Design. *Microelectron. Reliab.* **2014**, *54*, 1935−1939.

https://dx.doi.org/10.1021/acsami.0c01594
ACS Appl. Mater. Interfaces 2020, 12, 24419−24431

(6) Takata, Y.; Hidaka, S.; Uraguchi, T. Boiling Feature on a Super Water-Repellent Surface. *Heat Transfer Eng.* **2006**, *27*, 25−30.
(7) Hsu, C.-C.; Chen, P.-H. Surface Wettability Effects on Critical Heat Flux of Boiling Heat Transfer Using Nanoparticle Coatings. *Int. J. Heat Mass Transfer* **2012**, *55*, 3713−3719.
(8) Zupančič, M.; Steinbücher, M.; Gregorčič, P.; Golobič, I. Enhanced Pool-Boiling Heat Transfer on Laser-Made Hydrophobic/Superhydrophilic Polydimethylsiloxane-Silica Patterned Surfaces. *Appl. Therm. Eng.* **2015**, *91*, 288−297.
(9) Lv, Y.; Liu, M. Y.; Hui, L. F.; Pavlenko, A. N.; Surtaev, A. S.; Serdyukov, V. S. Heat Transfer and Fouling Rate at Boiling on Superhydrophobic Surface with TiO 2 Nanotube-Array Structure. *J. Eng. Thermophys.* **2019**, *28*, 163−176.
(10) Surtaev, A. S.; Serdyukov, V. S.; Safonov, A. I. Enhancement of Boiling Heat Transfer on Hydrophobic Fluoropolymer Coatings. *Interfacial Phenom. Heat Transfer* **2018**, *6*, 269−276.
(11) Allred, T. P.; Weibel, J. A.; Garimella, S. V. The Petal Effect of Parahydrophobic Surfaces Offers Low Receding Contact Angles That Promote Effective Boiling. *Int. J. Heat Mass Transfer* **2019**, 403−412.
(12) Motezakker, A. R.; Sadaghiani, A. K.; Çelik, S.; Larsen, T.; Villanueva, L. G.; Koşar, A. Optimum Ratio of Hydrophobic to Hydrophilic Areas of Biphilic Surfaces in Thermal Fluid Systems Involving Boiling. *Int. J. Heat Mass Transfer* **2019**, *135*, 164−174.
(13) Young Lee, C.; Hossain Bhuiya, M. M.; Kim, K. J. Pool Boiling Heat Transfer with Nano-Porous Surface. *Int. J. Heat Mass Transfer* **2010**, *53*, 4274−4279.
(14) Xu, P.; Li, Q.; Xuan, Y. Enhanced Boiling Heat Transfer on Composite Porous Surface. *Int. J. Heat Mass Transfer* **2015**, *80*, 107−114.
(15) Takata, Y.; Hidaka, S.; Masuda, M.; Ito, T. Pool Boiling on a Superhydrophilic Surface. *Int. J. Energy Res.* **2003**, *27*, 111−119.
(16) Anderson, T. M.; Mudawar, I. Microelectronic Cooling by Enhanced Pool Boiling of a Dielectric Fluorocarbon Liquid. *J. Heat Transfer* **1989**, *111*, 752−759.
(17) Dashi, S.; Yong, T.; Biao, T. Enhanced Boiling Microstructures Applied to Microelectronics Cooling. *2009 Int. Conf. Meas. Technol. Mechatronics Autom. ICMTMA 2009*; IEEE: 2009, *3*, 380−383. DOI: 10.1109/ICMTMA.2009.612.
(18) Allred, T. P.; Weibel, J. A.; Garimella, S. V. Enabling Highly Effective Boiling from Superhydrophobic Surfaces. *Phys. Rev. Lett.* **2018**, 174501.
(19) Liang, G.; Mudawar, I. Review of Pool Boiling Enhancement by Surface Modification. *Int. J. Heat Mass Transfer* **2019**, *128*, 892−933.
(20) Mori, S.; Utaka, Y. Critical Heat Flux Enhancement by Surface Modification in a Saturated Pool Boiling: A Review. *Int. J. Heat Mass Transfer* **2017**, *108*, 2534−2557.
(21) Li, J.; Fu, W.; Zhang, B.; Zhu, G.; Miljkovic, N. Ultrascalable Three-Tier Hierarchical Nanoengineered Surfaces for Optimized Boiling. *ACS Nano* **2019**, 14080.
(22) Rahman, M. M.; Ölçeroğğlu, E.; McCarthy, M. Scalable Nanomanufacturing of Virus-Templated Coatings for Enhanced Boiling. *Adv. Mater. Interfaces* **2014**, *1*, 1300107.
(23) Gregorčič, P.; Zupančič, M.; Golobič, I. Scalable Surface Microstructuring by a Fiber Laser for Controlled Nucleate Boiling Performance of High- and Low-Surface-Tension Fluids. *Sci. Rep.* **2018**, *8*, 7461.
(24) Gregorčič, P.; Šetina-Batič, B.; Hočevar, M. Controlling the Stainless Steel Surface Wettability by Nanosecond Direct Laser Texturing at High Fluences. *Appl. Phys. A: Mater. Sci. Process.* **2017**, *123*, 766.
(25) Gregorčič, P. Comment on "Bioinspired Reversible Switch between Underwater Superoleophobicity/Superaerophobicity and Oleophilicity/Aerophilicity and Improved Antireflective Property on the Nanosecond Laser-Ablated Superhydrophobic Titanium Surfaces". *ACS Appl. Mater. Interfaces* **2020**, DOI: 10.1021/acsami.9b23462.
(26) Kruse, C. M.; Anderson, T.; Wilson, C.; Zuhlke, C.; Alexander, D.; Gogos, G.; Ndao, S. Enhanced Pool-Boiling Heat Transfer and Critical Heat Flux on Femtosecond Laser Processed Stainless Steel Surfaces. *Int. J. Heat Mass Transfer* **2015**, *82*, 109−116.
(27) Nirgude, V. V.; Sahu, S. K. Enhancement in Nucleate Pool Boiling Heat Transfer on Nano-Second Laser Processed Copper Surfaces. *Exp. Heat Transfer* **2018**, *32*, 566−583.
(28) Zupančič, M.; Može, M.; Gregorčič, P.; Golobič, I. Nanosecond Laser Texturing of Uniformly and Non-Uniformly Wettable Micro Structured Metal Surfaces for Enhanced Boiling Heat Transfer. *Appl. Surf. Sci.* **2017**, *399*, 480−490.
(29) Voglar, J.; Gregorčič, P.; Zupančič, M.; Golobič, I. Boiling Performance on Surfaces with Capillary-Length-Spaced One- and Two-Dimensional Laser-Textured Patterns. *Int. J. Heat Mass Transfer* **2018**, *127*, 1188−1196.
(30) Može, M.; Zupančič, M.; Hočevar, M.; Golobič, I.; Gregorčič, P. Surface Chemistry and Morphology Transition Induced by Critical Heat Flux Incipience on Laser-Textured Copper Surfaces. *Appl. Surf. Sci.* **2019**, *490*, 220−230.
(31) Zakšek, P.; Zupančič, M.; Gregorčič, P.; Golobič, I. Investigation of Nucleate Pool Boiling of Saturated Pure Liquids and Ethanol-Water Mixtures on Smooth and Laser-Textured Surfaces. *Nanoscale Microscale Thermophys. Eng.* **2020**, *24*, 29−42.
(32) Gregorčič, P.; Conradi, M.; Hribar, L.; Hočevar, M. Long-Term Influence of Laser-Processing Parameters on (Super)Hydrophobicity Development and Stability of Stainless-Steel Surfaces. *Materials* **2018**, *11*, 2240.
(33) Long, J.; Cao, Z.; Lin, C.; Zhou, C.; He, Z.; Xie, X. Formation Mechanism of Hierarchical Micro- and Nanostructures on Copper Induced by Low-Cost Nanosecond Lasers. *Appl. Surf. Sci.* **2019**, *464*, 412−421.
(34) Chavan, S.; Park, D.; Singla, N.; Sokalski, P.; Boyina, K.; Miljkovic, N. Effect of Latent Heat Released by Freezing Droplets during Frost Wave Propagation. *Langmuir* **2018**, *34*, 6636−6644.
(35) Barthlott, W.; Neinhuis, C. Purity of the Sacred Lotus, or Escape from Contamination in Biological Surfaces. *Planta* **1997**, *202*, 1−8.
(36) Kietzig, A.-M.; Negar Mirvakili, M.; Kamal, S.; Englezos, P.; Hatzikiriakos, S. G. Laser-Patterned Super-Hydrophobic Pure Metallic Substrates: Cassie to Wenzel Wetting Transitions. *J. Adhes. Sci. Technol.* **2011**, *25*, 2789−2809.
(37) Groenendijk, M. Fabrication of Super Hydrophobic Surfaces by Fs Laser Pulses. *Laser Tech. J.* **2008**, *5*, 44−47.
(38) Conradi, M.; Drnovšek, A.; Gregorčič, P. Wettability and Friction Control of a Stainless Steel Surface by Combining Nanosecond Laser Texturing and Adsorption of Superhydrophobic Nanosilica Particles. *Sci. Rep.* **2018**, *8*, 7457.
(39) Boinovich, L. B.; Modin, E. B.; Aleshkin, A. V.; Emelyanenko, K. A.; Zulkarneev, E. R.; Kiseleva, I. A.; Vasiliev, A. L.; Emelyanenko, A. M. Effective Antibacterial Nanotextured Surfaces Based on Extreme Wettability and Bacteriophage Seeding. *ACS Appl. Nano Mater.* **2018**, *1*, 1348−1359.
(40) Emelyanenko, A. M.; Shagieva, F. M.; Domantovsky, A. G.; Boinovich, L. B. Nanosecond Laser Micro- and Nanotexturing for the Design of a Superhydrophobic Coating Robust against Long-Term Contact with Water, Cavitation, and Abrasion. *Appl. Surf. Sci.* **2015**, *332*, 513−517.
(41) Conradi, M.; Sever, T.; Gregorčič, P.; Kocijan, A. Short- and Long-Term Wettability Evolution and Corrosion Resistance of Uncoated and Polymer-Coated Laser-Textured Steel Surface. *Coatings* **2019**, *9*, 592.
(42) Arkles, B.; Pan, Y.; Larson, G. L.; Singh, M. Enhanced Hydrolytic Stability of Siliceous Surfaces Modified with Pendant Dipodal Silanes. *Chem. - Eur. J.* **2014**, *20*, 9442−9450.
(43) Yang, Z.; Wu, Y.-Z.; Ye, Y.-F.; Gong, M.-G.; Xu, X.-L. A Simple Way to Fabricate an Aluminum Sheet with Superhydrophobic and Self-Cleaning Properties. *Chin. Phys. B* **2012**, *21*, 126801.
(44) Xia, D.; Johnson, L. M.; López, G. P. Anisotropic Wetting Surfaces with One-Dimesional and Directional Structures: Fabrication Approaches, Wetting Properties and Potential Applications. *Adv. Mater.* **2012**, *24*, 1287−1302.

(45) Tawfick, S.; De Volder, M.; Copic, D.; Park, S. J.; Oliver, C. R.; Polsen, E. S.; Roberts, M. J.; Hart, A. J. Engineering of Micro- and Nanostructured Surfaces with Anisotropic Geometries and Properties. *Adv. Mater.* **2012**, *24*, 1628−1674.
(46) Alwitt, R. S. The Growth of Hydrous Oxide Films on Aluminum. *J. Electrochem. Soc.* **1974**, *121*, 1322−1328.
(47) Din, R. U.; Yuksel, S.; Jellesen, M. S.; Møller, P.; Ambat, R. Steam Assisted Accelerated Growth of Oxide Layer on Aluminium Alloys. In *Proceedings of Eurocorr 2013;* European Federation of Corrosion: 2013, *1090*, 1−7.
(48) Min, J.; Webb, R. L. Long-Term Wetting and Corrosion Characteristics of Hot Water Treated Aluminum and Copper Fin Stocks. *Int. J. Refrig.* **2002**, *25*, 1054−1061.
(49) Betz, A. R.; Xu, J.; Qiu, H.; Attinger, D. Do Surfaces with Mixed Hydrophilic and Hydrophobic Areas Enhance Pool Boiling? *Appl. Phys. Lett.* **2010**, *97*, 141909.
(50) Rahman, M. M.; Ölçeroğlu, E.; McCarthy, M. Role of Wickability on the Critical Heat Flux of Structured Superhydrophilic Surfaces. *Langmuir* **2014**, *30*, 11225−11234.
(51) Griffith, P.; Wallis, J. D. *The Role of Surface Conditions in Nucleate Boiling*; Cambridge, Mass.: Massachusetts Institute of Technology, Division of Industrial Cooperation: 1958, pp 49−63.
(52) Rohsenow, W. M. Nucleation with Boiling Heat Transfer. *Ind. Eng. Chem.* **1966**, *58*, 40−47.
(53) Hsu, Y. Y. On the Size Range of Active Nucleation Cavities on a Heating Surface. *J. Heat Transfer* **1962**, *84*, 207−213.
(54) Shoukri, M.; Judd, R. L. Nucleation Site Activation in Saturated Boiling. *J. Heat Transfer* **1975**, *97*, 93−98.
(55) Vargel, C. *Corrosion of Aluminium*; Elsevier B.V.: 2004. DOI: 10.1016/B978-0-08-044495-6.X5000-9.
(56) Diggle, J. W.; Vijh, A. K. *Oxides and Oxide Films*; Marcel Dekker, 1976; Vol. *4*.
(57) Preckshot, G. W.; Denny, V. E. Explorations of Surface and Cavity Properties on the Nucleate Boiling of Carbon Tetrachloride. *Can. J. Chem. Eng.* **1967**, *45*, 241−246.
(58) Turnbull, D. Kinetics of Heterogeneous Nucleation. *J. Chem. Phys.* **1950**, *18*, 198−203.
(59) Carey, V. P. *Liquid-Vapor Phase-Change Phenomena: An Introduction to the Thermophysics of Vaporization and Condensation Processes in Heat Transfer Equipment*; CRC Press: 2020, DOI: 10.1201/9780429082221.
(60) Bankoff, S. G. Ebullition From Solid Surfaces in the Absence of a Pre-Existing Gaseous Phase. *Trans. Am. Soc. Mech. Eng.* **1957**, *79*, 735−740.
(61) Cole, R. Boiling Nucleation. *Adv. in Heat Transfer* **1974**, *10*, 85−166.
(62) Qi, Y.; Klausner, J. F.; Mei, R. Role of Surface Structure in Heterogeneous Nucleation. *Int. J. Heat Mass Transfer* **2004**, 3097−3107.
(63) Shen, B.; Yamada, M.; Hidaka, S.; Liu, J.; Shiomi, J.; Amberg, G.; Do-Quang, M.; Kohno, M.; Takahashi, K.; Takata, Y. Early Onset of Nucleate Boiling on Gas-Covered Biphilic Surfaces. *Sci. Rep.* **2017**, *7*, 2036.
(64) Kruse, C.; Peng, E.; Zuhlke, C.; Shield, J.; Alexander, D.; Ndao, S.; Gogos, G. Role of Copper Oxide Layer on Pool Boiling Performance with Femtosecond Laser Processed Surfaces. In *ASME 2017 15th International Conference on Nanochannels, Microchannels, and Minichannels;* American Society of Mechanical Engineers Digital Collection: 2017.
(65) Kruse, C.; Tsubaki, A.; Zuhlke, C.; Alexander, D.; Anderson, M.; Peng, E.; Shield, J.; Ndao, S.; Gogos, G. Influence of Copper Oxide on Femtosecond Laser Surface Processed Copper Pool Boiling Heat Transfer Surfaces. *J. Heat Transfer* **2019**, *141*, No. 051503.
(66) Mani, D.; Sivan, S.; Ali, H. M.; Ganesan, U. K. Investigation to Improve the Pool Boiling Heat Transfer Characteristics Using Laser-Textured Copper-Grooved Surfaces. *Int. J. Photoenergy* **2020**, *2020*, 3846157.
(67) Marmur, A.; Della Volpe, C.; Siboni, S.; Amirfazli, A.; Drelich, J. W. Contact Angles and Wettability: Towards Common and Accurate Terminology. *Surf. Innovations* **2017**, *5*, 3−8.
(68) Može, M.; Zupančič, M.; Golobič, I. Investigation of the Scatter in Reported Pool Boiling CHF Measurements Including Analysis of Heat Flux and Measurement Uncertainty Evaluation Methodology. *Appl. Therm. Eng.* **2020**, *169*, 114938.

https://dx.doi.org/10.1021/acsami.0c01594
ACS Appl. Mater. Interfaces 2020, 12, 24419−24431